An Animal Virus-Derived Peptide Switches Membrane Morphology: Possible Relevance to Nodaviral Transfection Processes†

Andreas Janshoff,‡,§ Dennis T. Bong,‡,§ Claudia Steinem,‡,§ John E. Johnson,§ and M. Reza Ghadiri*,‡,§

Departments of Chemistry and Molecular Biology and Skaggs Institute for Chemical Biology, The Scripps Research Institute, La Jolla, California 92037

Received December 17, 1998; Revised Manuscript Received February 24, 1999

ABSTRACT: The N-terminal domain of the capsid protein cleavage product of the flock house virus (FHV) consists of 21 residues and forms an amphipathic α-helix, which is thought to play a crucial role in permeabilizing biological membranes for RNA translocation in the host cell. We have found that the Met → Nle variant of this domain (denoted here as γ_1) efficiently induces the formation of the interdigitated gel phase ($L_\beta I$) of 1,2-dipalmitoyl-*sn*-glycero-3-phosphatidylcholine (DPPC) bilayers. In situ scanning force microscopy of solid supported bilayers and fluorescence spectroscopy of peptide-treated DPPC vesicles provide evidence for the formation of acyl chain interdigitated lipid domains. It could be shown by fluorescence spectroscopy that the peptide inserts in the DPPC matrix above the main transition temperature of the lipid, while the formation of domains with decreased thickness occurs after the sample is cooled to 25 °C. The orientation and secondary structure of the peptide in lipid bilayers were investigated using attenuated total reflectance infrared (ATR-IR) and circular dichroism (CD) spectroscopy. These results enabled us to formulate a mechanistic model for the peptide-mediated induction of interdigitation in DPPC bilayers. Moreover, the membrane activity of γ_1 with gel phase lipids established in this study may have further implications for the infection strategy adopted by simple RNA viruses.

Nodaviruses are simple nonenveloped RNA animal viruses composed of a single gene product capsid protein that packages a bipartite single-stranded RNA genome (*5*). The relative simplicity of these icosahedral viruses renders them attractive systems for the study of fundamental aspects of viral lifecycles (*6*). A central process of the nodaviral life cycle, the transfection process, has as yet not been well-elucidated. However, high-resolution structural investigation (*6*, *7*) of the flock house nodavirus (FHV)[1] and related viruses (*8*) has led to the intriguing hypothesis that a C-terminal capsid protein cleavage product, called the γ-peptide in FHV, plays a pivotal membrane-permeabilizing role that facilitates RNA−virion translocation. We have established that the 21 N-terminal residues (denoted γ_1, Scheme 1) of the 44-residue γ-peptide do indeed bind to fluid phase membranes with high avidity and also induce dramatic increases in liposomal bilayer permeability (*9*). We report herein that synthetic γ_1 also exerts a unique effect on neutral gel phase lipids; treatment of dipalmitoylphosphatidylcholine (DPPC) bilayers

Scheme 1: Helical Wheel Representation of the γ_1-Peptide[a]

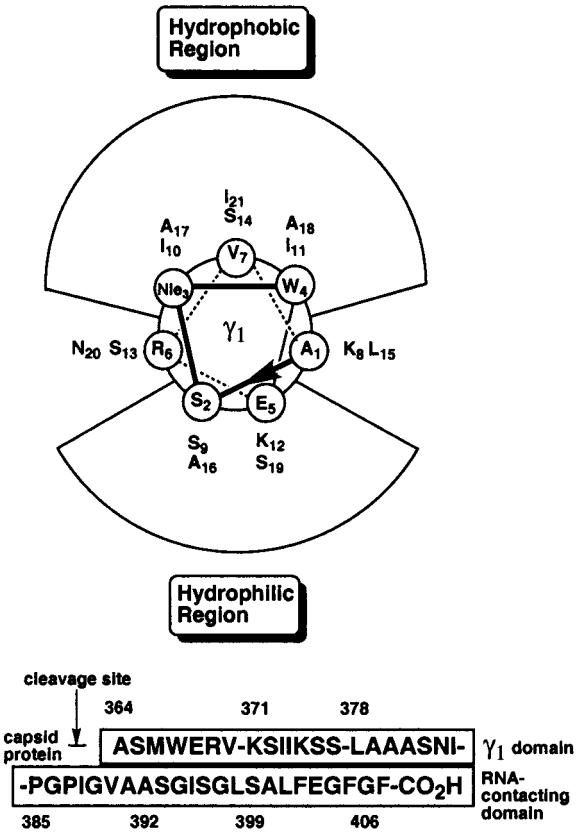

[a] The numbered sequence of the entire γ-peptide is shown, with the cleavage site denoted with an arrow and helical and RNA contacting portions denoted as boxed regions.

† We thank the Skaggs Institute for Chemical Biology for the primary financial support of this program and also the Fonds der Chemischen Industrie (A.J.) and the DFG (C.S.) for postdoctoral fellowships.

* Author to whom correspondence should be addressed.

‡ Department of Chemistry and Skaggs Institute for Chemical Biology.

§ Department of Molecular Biology.

[1] Abbreviations: ATR-IR, attenuated total reflectance infrared; CD, circular dichroism; DMF, dimethylformamide; DPPC, 1,2-dipalmitoyl-*sn*-glycero-3-phosphocholine; FHV, flock house virus; LUVs, large unilamellar vesicles; L_α, lamellar liquid crystalline phase; $L_{\beta'}$, lamellar gel phase; $L_\beta I$, lamellar gel interdigitated phase; MBHA, methylbenzhydrylamine; PC, phosphocholine; PG, phosphoglycerol; PyrPC, 1-hexadecanoyl-2-(1-pyrenedecanoyl)-*sn*-glycero-3-phosphocholine; T_m, main (gel to liquid crystal) transition temperature; SFM, scanning force microscopy.

10.1021/bi982976i CCC: $18.00
Published on Web 04/02/1999

with low mole fractions of γ_1 results in a widespread change in morphology consistent with acyl chain interdigitation of gel phase phospholipids.

Interdigitation demands a drastic alteration of lipid packing in which the acyl chains of each monolayer extend across the membrane midplane to pack terminal methyl groups near the headgroups of the opposite lipid layer. As a result, an interdigitated membrane is much thinner and more closely packed (*10*) than a normal bilayer. Additionally, formation of these domains within bilayers has the functional consequence of increased membrane permeability to hydrophilic solutes (*11*, *12*), presumably because of hydrophobic mismatch at the boundary between bilayer and interdigitated regions. Lipid interdigitation can be induced by small organic molecules such as short chain alcohols, polyols, and the anesthetics chlorpromazine and tetracaine as well as by larger biomolecules such as myelin basic protein and polymyxin (*10*, *13*−*18*). Common features of these substances are their amphiphilic nature and their ability to replace water molecules bound to the headgroups of the phospholipids.

Above a critical concentration of amphiphilic inducer, the interdigitated ($L_\beta I$) phase becomes thermodynamically preferred over the normal bilayer gel phase ($L_{\beta'}$), partly as a result of enhanced van der Waals contacts and reduced steric crowding of the PC headgroups in the $L_\beta I$ phase. Active amphiphiles are able to offset the thermodynamic cost of exposing the fatty acid methylene groups to the aqueous environment by binding to the hydrophobic sites, thus replacing water at these sites with both enthalpic and entropic benefit. According to Rowe et al. (*19*), the interdigitated $L_\beta I$ phase replaces the ripple phase $P_{\beta'}$, and thus occurs between the premelting ($L_{\beta'} \rightarrow P_{\beta'}$) and main phase transition ($P_{\beta'}/L_\beta I \rightarrow L_\alpha$) in the thermotropic profile of DPPC. Accordingly, the interdigitated phase ($L_\beta I$) has not been observed for lipids in the fluid phase; the bilayer must be in the gel phase for interdigitation to occur (*4*).

This study presents a biophysical picture of the mode of interaction of the FHV cleavage peptide fragment with gel phase membranes using scanning force microscopy, ATR-IR, fluorescence spectroscopy, and circular dichroism (CD) measurements. Scanning force microscopy with supported DPPC bilayers has revealed that γ_1 causes depressions in the lipid bilayer; the occurrence of these phase-separated thinner domains increases with increasing peptide concentrations. Furthermore, section analysis of the bilayer correlates well with previously reported height profiles of interdigitated domains induced by ethanol in DPPC bilayers (*20*). In conjunction with pyrene excimer fluorescence experiments (*21*), these membrane profiles suggest the induction of interdigitated lipid phases by γ_1-peptide. Thus, these results depict a peptide that effectively binds gel phase lipids and induces gross morphological changes in membrane structure and properties, providing further support for the hypothesized membrane-permeabilizing role of the γ-peptide of the flock house virus.

MATERIALS AND METHODS

Materials. 1,2-Dipalmitoyl-*sn*-glycero-3-phosphocholine (DPPC) was purchased from Avanti Polar Lipids (Alabaster, AL), and 1-hexadecanoyl-2-(1-pyrenedecanoyl)-*sn*-glycero-3-phosphocholine (PyrPC) was purchased from Molecular Probes (Eugene, OR). Methanol and chloroform were of HPLC and optima grade, respectively, and were obtained from Fisher Scientific. Punctillious 200 proof ethanol was obtained from Quantum Chemical Co. All lipids and solvents were used as purchased without further purification.

Peptide Synthesis. Manual Boc solid phase peptide synthesis of γ_1 was carried out according to the in situ neutralization protocol of Kent (*22*) with HBTU activation and employing methylbenzhydrylamine (MBHA) resin (0.56 mequiv/g loading). Formyl protection on tryptophan was removed prior to resin cleavage by treatment of the peptide−resin with 10% hydrazine−monohydrate in DMF at 0 °C for 8 h. The peptide was cleaved from resin using standard HF procedures and eluted from the resin with TFA following washing with ethyl ether. The resulting free peptide solution was lyophilized, redissolved in acidic water/acetonitrile, and purified by reverse phase high-performance liquid chromatography on a Vydac C_{18} column using a CH_3CN/H_2O/TFA gradient. Methionine was replaced with norleucine in the synthesis to avoid problems of spontaneous oxidation of the methionine thioether side chain. The peptide used in all measurements thus bears this substitution, as well as a free N-terminus, as in the native γ-peptide, and a C-terminal primary amide resulting from cleavage from MBHA resin.

Liposome Preparation. Lipids were used as purchased to prepare films of 1,2-dipalmitoyl-*sn*-glycero-3-phosphocholine (DPPC) by drying the lipid dissolved in chloroform under a stream of nitrogen while heating above the main phase transition temperature T_m of DPPC ($T_m = 41.5$ °C), followed by several hours under vacuum. Multilamellar vesicles were prepared by swelling the lipid film in aqueous solution while incubating at 65 °C for 30 min with periodic vortexing for 30 s. For the fluorescence, CD, and excimer experiments, liposomes were prepared in 100 mM phosphate buffer at pH 7.0; for the ATR-IR and AFM study, the lipids were swelled with doubly distilled water and 20 mM NaCl (pH 5.6), respectively. The resulting multilamellar vesicles were then sized at 65 °C by extrusion through stacked polycarbonate membranes with pore diameters of approximately 200 nm using a miniextruder (LiposoFast, Avestin) to obtain large unilamellar vesicles (LUVs). For the excimer fluorescence experiments, DPPC films containing 10 mol % PyrPC were used instead of pure DPPC films. The lipid concentration was determined after extrusion by lyophilization of a known volume of the LUV suspension and analysis of the resulting powder by ^{1}H NMR, using dioxane or benzene as an internal standard for peak integration. An acquisition delay of 15 s was used to ensure integration accuracy. The concentration of the fluorescence probe was assayed by UV absorption measurements on the same sample, using an extinction coefficient of 41 700 M^{-1} cm^{-1} at $\lambda = 341$ nm. The peptide concentration was determined by UV spectroscopy assuming an extinction coefficient of 5570 M^{-1} cm^{-1} at $\lambda = 280$ nm.

Preparation of Peptide−Liposome Complexes. In all cases, an aqueous solution of peptide was mixed with preformed DPPC liposome suspensions and incubated for 30 min to 1 h above the main phase transition temperature of DPPC. The samples were then equilibrated to 25 °C prior to measurements being carried out at the same temperature.

Circular Dichroism Spectroscopy. Circular dichroism (CD) spectra were obtained using an Aviv 62DS (Lakewood, NJ) spectrograph. Samples were scanned in a 0.2 cm CD cell

from 260 to 190 nm with 0.1 nm resolution and 1 nm bandwidth in a water-jacketed sample chamber thermostated at 25 °C. Ellipticity is reported as mean residue ellipticity in degrees per square centimeter per decimole. DPPC LUVs were added to a 20−50 μM peptide solution for CD measurements; spectra were background-corrected for light scattering and buffer absorption. Reported CD spectra are the average of six wavelength scans. Spectra were deconvoluted to determine secondary structure content using a neural network-based deconvolution algorithm (*23*−*25*) (CDNN 2.1) and α-helix estimation at $\lambda_{min} = 208$ and 222 nm.

Fluorescence Measurements. All fluorescence emission measurements were performed on an Aminco/Bowman luminescence spectrometer equipped with a water-jacketed sample chamber thermostated at 25 °C.

Tryptophan Fluorescence Measurements. Fluorescence spectra of mixtures of DPPC LUVs and γ_1 were recorded before and after heating the sample to 50 °C and incubation for 30 min. The tryptophan fluorescence was monitored from 300 to 450 nm with excitation at 280 nm and a 4 nm band-pass through a 300 nm low-pass filter (Hoya Optics). Experiments probing the efficiency of collisional quenching of tryptophan by CsCl were conducted at a lipid:peptide ratio of 150:1. Varying amounts of an aqueous CsCl solution were added after room-temperature equilibration to yield samples in which the final cesium concentrations ranged from 0 to 0.5 M. Additional NaCl was added to bring the total salt concentration to a constant value for all samples.

Excimer Fluorescence Measurements. Pyrene-containing samples were excited at 341 nm, and emission was monitored from 360 to 600 nm with a 4 nm band-pass. Excimer/monomer ratios were calculated from the fluorescence intensity ratio of the respective emission bands at 477 and 377 nm.

FT-ATR-IR Spectroscopy. Oriented lipid multibilayers were prepared by drying 500 μL of a DPPC LUV−peptide suspension (lipid concentration of 2 mg/mL, lipid:peptide ratio of 150:1) on a germanium crystal ($\theta = 45°$, Spectra-Tech) under a nitrogen atmosphere. Spectra were acquired under a dry nitrogen atmosphere at 4 cm^{-1} resolution on a Nicolet 550 Magna Series II FT-IR instrument equipped with a liquid nitrogen-cooled mercury−cadmium telluride detector. A baseline horizontal ATR optical bench holding the germanium crystal (Spectra-Tech) and a ZnSe polarizer (Spectra-Tech) were used in the spectrometer. Reported spectra are the average of 800 scans taken with either parallel or perpendicular polarized light.

Calculation of Orientation. The IR dichroism of peptide amide I (1656 cm^{-1}, C═O stretch) and lipid symmetric CH_2 (2850 cm^{-1}) stretching vibrations were used to gauge the molecular orientation in each sample. Orientation information was extracted from dichroic ratios by following published methods (*26*−*30*). The dichroic ratio R is defined as the ratio of absorption of incident IR light plane-polarized parallel to the surface normal ($A_{||}$) to that of light plane-polarized perpendicular to the surface normal ($A_{\perp}$). Ratios used in orientation calculations were the average of at least four measurements. Peaks in the amide I region were decomposed with Lorentzian/Gaussian functions (0.5:0.5) to accurately determine discrete absorption intensities in the spectra of the peptide−DPPC multibilayers. The angle between the α-helix axis and the transition dipole moment of the amide I transition was assumed to be 39°, whereas the angle between the lipid CH_2 transition dipole moment and the acyl chain axis was set to 90° (*31*). The refractive indices of the germanium crystal and lipid film are 4.03 and 1.5, respectively. The angle between the surface normal and the molecular axis of the α-helix was determined using necessary corrections for the α-helical content of γ_1, as determined by CD measurements of γ_1 incorporated in liposomes.

Preparation of Solid Supported Lipid Bilayers for SFM Analysis. Pure single DPPC bilayers were spread on mica substrates using a modified version (*20*) of the vesicle fusion method (*32*). Briefly, a suspension of unilamellar DPPC vesicles (0.5 mg/mL) in 20 mM NaCl was applied to a freshly cleaved mica sheet at room temperature. After 10 h at 4 °C, the bilayer was formed by incubating the sealed sample at 50 °C for 30 min. The solid supported lipid bilayers were imaged after extensive washing to remove adsorbed vesicles with aqueous 20 mM NaCl. Incorporation of the peptide into supported membranes was accomplished either by incubating peptide solution with the spread bilayer at 65 °C for 30 min or by spreading liposomes which had been treated with peptide as previously described. Similar results were obtained with each method, though the degree of interdigitation was more reproducible when the bilayer was formed from pretreated vesicles.

Scanning Force Microscopy. Surface images of the solid supported lipid bilayers were obtained in an open fluid chamber using a Nanoscope IIIa Multimode scanning probe microscope (Digital Instruments, Santa Barbara, CA) operating in TappingMode (in fluids) and contact mode, equipped with a 15 μm × 15 μm scanner (E-scanner). Height values were the average of 50 measurements. Line scans were baseline corrected if necessary by subtracting the slope and measuring the height differences between plateau regions. Microfabricated oxide-sharpened silicon nitride tips (NP-S, Digital Instruments) with an approximate spring constant of 0.06 N/m and a tip radius of 5−20 nm were used as purchased. Minimal load force (1−3 nN) was employed during contact mode imaging, while the scan rate was set as high as possible (4−7 Hz) to reduce the extent of bilayer deformation. The most reproducible results were obtained when mica substrates were fixed to Teflon-coated sample holders. This procedure ensures that the aqueous sample droplet placed on the mica sheet remains on the sample. To check for errors resulting from indentation of the bilayer by the load force tip, we additionally employed dynamic force microscopy (TappingMode) in solution, which confirmed the height information obtained from contact mode SFM within the error of the measurement.

RESULTS

Circular Dichroism Spectroscopy. The interaction of γ_1 with DPPC liposomes was studied by observing the change in ellipticity upon adding unilamellar vesicles to the peptide dissolved in water or buffer. The γ_1-peptide fragment adopts a predominantly (40%) random coil conformation with low α-helical content (18%) in buffered solution (Figure 1). Addition of DPPC LUVs at a 30:1 lipid:peptide ratio without heating above the T_m of DPPC resulted in a nominal increase in α-helicity (23−30%). However, incubation of the same

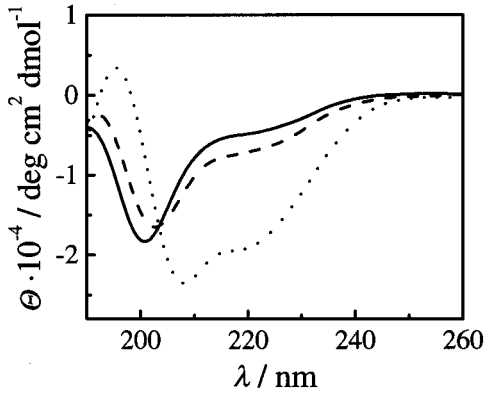

FIGURE 1: CD spectra (—) of the γ_1-peptide (4.5×10^{-5} M in 100 mM phosphate at pH 7.0) and after titration with liposomes at room temperature (− − −). The CD spectrum of γ_1 interacting with DPPC after (···) equilibrating the sample at 55 °C for 1 h and recording the CD spectrum at room temperature.

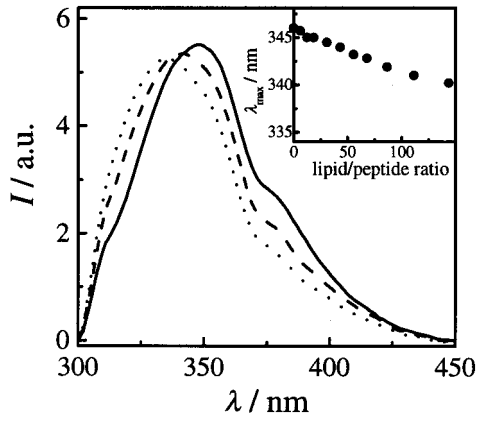

FIGURE 2: (—) Fluorescence emission spectra of a γ_1 solution (2.2×10^{-6} M) (− − −) after addition of DPPC LUVs (200 nm in diameter) at 25 °C and (···) after equilibrating the sample at 50 °C for 30 min. The inset shows the dependence of the emission wavelength maxima on the lipid:peptide ratio.

sample at 50 °C for 1 h and subsequent cooling to room temperature (25 °C) effected a considerable increase in the α-helix content of the peptide (62−70%). The CD spectrum did not change in the absence of lipid, indicating that peptide folding is induced by interaction with the hydrophobic lipid matrix. To probe the relative contributions of lipid headgroup and hydrophobic interactions to the conformational change of the γ_1-peptide, we also studied the effect of negatively charged DPPG vesicles on peptide secondary structure. At a DPPG:peptide ratio of 50:1, a substantial increase in the helix content (>50%) could be observed below the phase transition temperature of DPPG (T_m = 41 °C), indicating a strong electrostatic interaction between the positively charged peptide and the negatively charged headgroups of the lipid molecules (Supporting Information). Saturation of the organizational effect of the hydrophobic matrix was reached at a lipid:peptide ratio of approximately 80:1, yielding 70−76% peptide helicity. The helicity of the peptide therefore increases from approximately 20% in buffer to >70% in the DPPC matrix, in good agreement with secondary structure predictions (76%) and the maximum α-helicity (72−81%) obtained in a 50% TFE/buffer solution (*33*, *34*).

Tryptophan Emission Spectra. Tryptophan 4 in the γ_1 sequence provided a useful probe of the peptide dielectric environment. It has been shown (*35*) that the maximum fluorescence emission for tryptophan located near the headgroup region of a phospholipid bilayer is between 335 and 343 nm, whereas tryptophan residues buried in the hydrophobic region of the bilayer exhibit maximum fluorescence emission between 325 and 335 nm. The fluorescence spectrum of the γ_1-peptide in aqueous buffer exhibits an emission maximum at 348 nm (Figure 2). Stepwise addition of DPPC LUVs below the T_m leads to a 6 nm decrease in λ_{max}. However, incubation of the same lipid−peptide suspension at 50 °C for 30 min results in a considerable 13−15 nm blue shift of the emission maximum upon re-equilibration to 25 °C. This observation, consistent with the above CD studies, suggests that membrane incorporation of the peptide is only permissible when the bilayer is in the fluid state, though the helical peptide remains in the membrane with its hydrophobic face buried in the hydrocarbon interior when the lipids return to the gel phase. The mode of the γ_1-peptide−lipid bilayer interaction was further corroborated by aqueous phase collisional quenching fluorescence experiments. Cesium ions have low bilayer permeability, and thus, a hydrophobically buried tryptophan should be protected from collisional quenching. The Stern−Volmer quenching rate constant obtained for a free peptide solution (k = 1.8 M^{-1}) was larger than that obtained for a 150:1 DPPC−peptide complex (k = 0.8 M^{-1}), indicating that the tryptophan is indeed shielded from cesium in the bilayer interior.

FT-IR Spectroscopy. The location and intensity of amide bond vibrations in the regions of 1700−1500 and 3200−3500 cm^{-1} are highly diagnostic of peptide secondary structure and orientation relative to a surface normal. Fourier transform IR spectra of dried γ_1-peptide films on CaF_2 disks display maximum intensities at 1656 cm^{-1} (1684 and 1656 cm^{-1}) and 1546 cm^{-1} (1532 and 1547 cm^{-1}) which are assigned to the amide I and II vibrations, respectively (Figure 3A). An amide A band appearing at 3293 cm^{-1} (data not shown) is indicative of hydrogen bonding. FT-IR data combined with peptide film CD measurements (*31*) demonstrate that the γ_1-peptide adopts an α-helical conformation in the solid state.

Polarized ATR-IR spectroscopy of peptide−DPPC multibilayers supported on a germanium crystal allowed us to quantitatively evaluate peptide orientation in the DPPC environment. We first investigated the dependence of the lipid orientation on the peptide concentration. The average tilt angle of the lipid acyl chains in pure lipid bilayers is 29 ± 1° relative to the surface normal. This value compares well with previously published data (*29*, *31*) in the range of 25−30°. Incorporation of the peptide into DPPC multibilayers at a lipid:peptide ratio of 150:1 did not affect either the peak width and stretching frequency of lipid CH_2 groups or the lipid chain orientation relative to the surface normal. The IR dichroism observed in the amide I and II regions of DPPC−peptide multibilayers is depicted in Figure 3B. The average dichroic ratio R_{1656} value of 1.5 ± 0.1 (amide I, 1656 cm^{-1}) is commensurate with an order parameter S of −0.42 ± 0.1. The 70% α-helix content was accounted for in the orientation calculation, which revealed an average angle of 68 ± 4° between the molecular axis of the α-helix and the surface normal.

Excimer Fluorescence Measurements. It has been previously demonstrated (*36*, *37*) that the formation of an interdigitated lipid phase has the structural consequence of

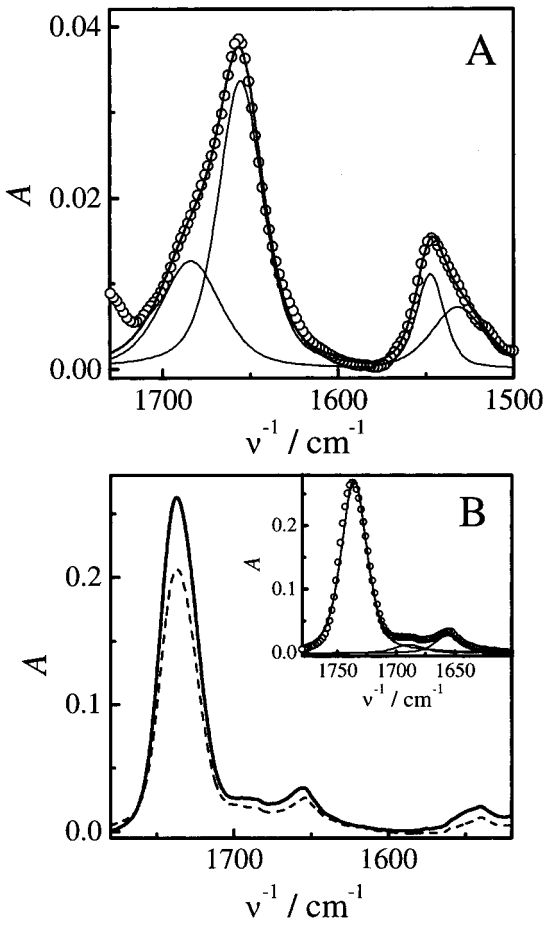

FIGURE 3: (A) Solid state transmission FT-IR absorbance spectrum of γ_1 on CaF_2 disks. The main bands at 1656 cm^{-1} (amide I) and 1546 cm^{-1} (amide II) indicate the α-helical conformation of the peptide. (B) Polarized FT-IR spectra of γ_1 in DPPC multibilayers (peptide:lipid ratio of 1:150) on a germanium crystal. The solid line represents the absorbance with incident light plane-polarized parallel to the surface normal and the dotted line with perpendicularly polarized light. The inset demonstrates the band decomposition of the parallel component. The individual fitted bands of mixed Lorentzian/Gaussian functions were integrated to obtain peak intensity. The sum and the component functions are shown as thick and thin solid lines, respectively.

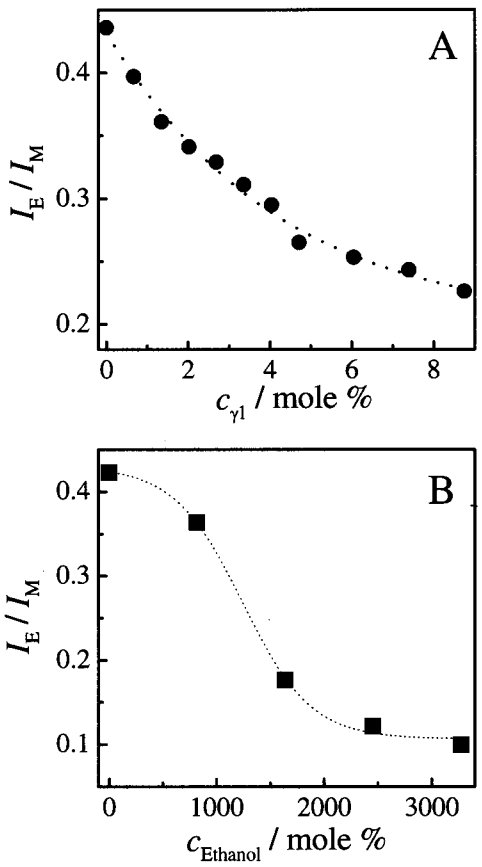

FIGURE 4: (A) Dependence of the pyrene excimer/monomer fluorescence ratio on the mole percent of γ_1 added to PyrPC-doped DPPC LUVs and (B) the dependence on the mole percent of ethanol.

rigidifying the membrane and decreasing lateral mobility within the bilayer; therefore, we sought to find evidence for attenuated lipid movement upon addition of peptide. To this end, 1-hexadecanoyl-2-(1-pyrenedecanoyl)-*sn*-glycero-3-phosphocholine (PyrPC) was used as a fluorescent probe to assay changes in membrane fluidity (*21*, *38*). Due to its similarity to DPPC, PyrPC is readily incorporated into DPPC bilayers without phase separation (*38*). The fluorescence signature of pyrene-functionalized lipid incorporated at a concentration of 10 mol % in DPPC liposomes features not only bands that arise from pyrene monomer but also an emission band from an excited state dimer, which forms via the collision of an excited state pyrene monomer and a ground state monomer (Supporting Information). As excimer formation depends on the collision of two species within the lipid membrane, the ratio of excimer/monomer (*E*/*M*) fluorescence intensity provides a sensitive measure of changes in lipid mobility (*21*, *38*). When unilamellar vesicle suspensions of DPPC containing 10 mol % PyrPC were treated with varying amounts of γ_1, a concentration-dependent decrease in *E*/*M* fluorescence intensity was observed (Figure 4A). This is similar to the fluorescence profile (Figure 4B) displayed when the same liposomes are treated with ethanol (*10*), or a number of other amphiphilic organic solvents known to cause lipid interdigitation (*16*), with the following significant differences. γ_1 is a much more potent agent for decreasing excimer fluorescence, and whereas the *E*/*M* fluorescence intensity displays a cooperative (sigmoidal) decrease with increasing ethanol concentrations, no cooperativity can be detected from the *E*/*M* dependency on peptide concentration.[2]

Scanning Force Microscopy. While decreases in lipid mobility provide good supporting evidence for interdigitation, direct substantiation of the interdigitation hypothesis can be obtained using scanning force microscopy. Examination of pure DPPC bilayers on mica surfaces using SFM revealed a flat, almost featureless surface; thus, bilayer height is the most defining characteristic. A commonly employed method for determining bilayer thickness requires application of a high load force to a small area (e.g., 500 nm × 500 nm) at high scanning velocities to remove the lipids from the scanned area (*39*). A subsequent scan of a larger area at low

[2] We also performed the same experiment with PyrPC-doped DPPG liposomes, which possess negatively charged headgroups. It has been reported that polymyxin B and polymyxin B nonapeptide both induce the interdigitated phase with DPPG bilayers (*1*, *2*); for comparison, we treated PyrPC−DPPG LUVs with polymyxin B nonapeptide in parallel with ethanol and γ_1. Our experiments revealed that the excimer/monomer ratio reflected a decrease in lipid mobility, though in both cases the changes were concomitant with liposome precipitation, complicating the interpretation of these results.

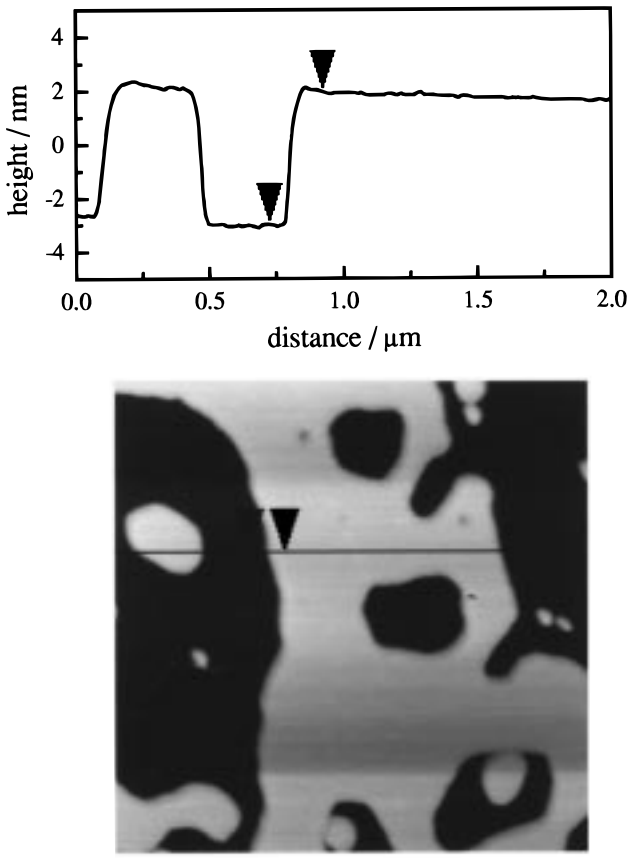

FIGURE 5: DPPC bilayer imaged by scanning force microscopy in contact mode. The image size is 2.6 μm × 2.6 μm. Large defects shown here were used to obtain a bilayer height profile. The thickness of the membrane was determined to be 5.6 nm. The lipid concentration was 0.5 mg/mL, buffered at pH 5.6 in 20 mM NaCl. The nominal spring constant of the cantilever was 0.06 N/m and the nominal tip radius 5−20 nm. The imaging force was approximately 2 nN and the scanning velocity 4 Hz.

imaging force and moderate scanning velocities then provides the desired height profile, which reveals the thickness of the membrane. However, we have found that this method often produces variable bilayer heights (±1 nm) depending on the length of the high-force scanning period, possibly as a result of partial destruction of the mica supporting substrate or incomplete lipid removal. To avoid this problem, we instead determined the bilayer thickness by measuring height profiles at the sites of large defects in the supported bilayer which result from the spreading procedure (Figure 5). The average bilayer thickness of 50 SFM measurements is 5.5 ± 0.2 nm, consistent with a DPPC bilayer and a thin layer of water between the mica surface and the membrane, as previously described (*20*). The effect of varying levels of γ_1 incorporation on the morphology of the supported membrane is shown in Figure 6. The formation of depressed domains (interdigitated lipid phase) in DPPC bilayers was observed. The height difference between the two kinds of lipid phases is about 1.5 ± 0.2 nm (Figure 7). Most significantly, increasing the amount of peptide led to an increase of the area occupied by the domains with smaller heights. Treatment of a DPPC bilayer with γ_1 at 0.02 mol % results in line-shaped domains, which comprise 2−6% of the bilayer surface area (Figure 6A). At a concentration of 0.1 mol % peptide, the supported membranes are phase separated with the thinner domains occupying 15−22% of the total area (Figure 6B). At 0.5 mol

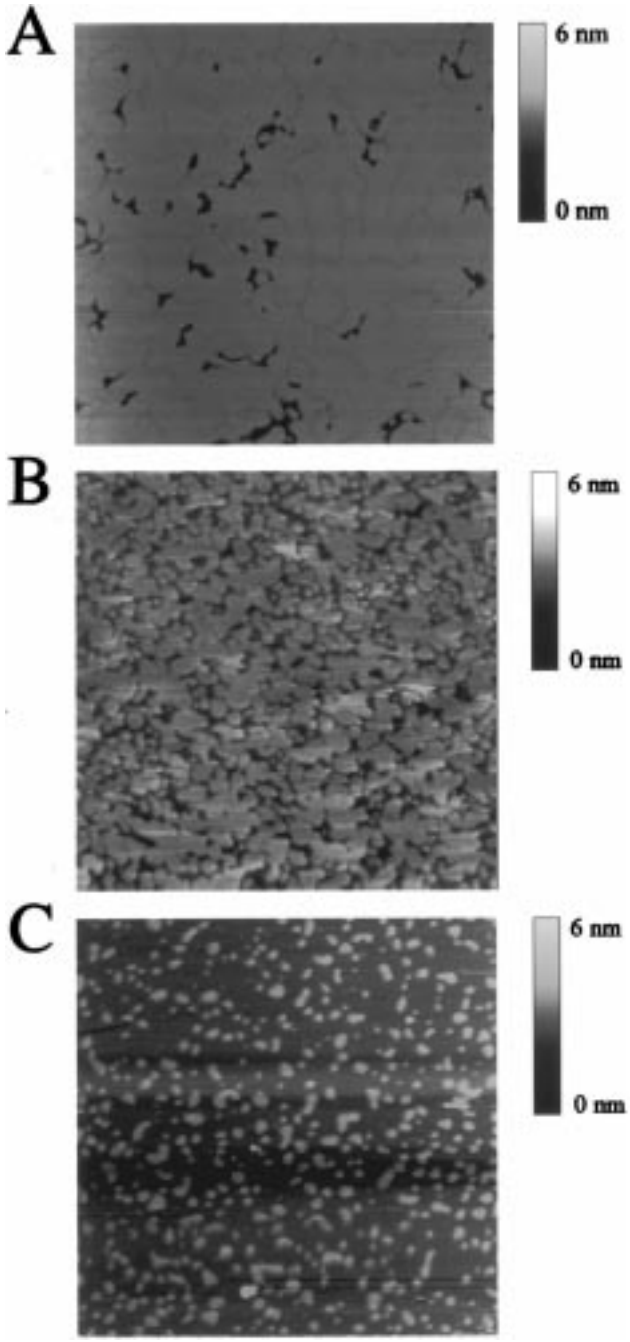

FIGURE 6: Formation of compressed domains in a DPPC bilayer on mica by treatment with increasing amounts of γ_1: (A) 0.02, (B) 0.1, and (C) 0.5 mol % γ_1. Imaged by SFM in contact mode (k = 0.06 N/m). The image size is 2.5 μm × 2.5 μm.

%, the area ratio of normal bilayer to compressed domains reverses, and the lower domains cover 80−90% of the surface (Figure 6C). Above 0.5 mol %, bilayer destruction and exclusively thinner membranes are observed. In addition, lateral force microscopy (Supporting Information) was employed to measure differences in friction of both domain surfaces. The images clearly reveal that even under high loading forces no noticeable differences in friction between the thinner and normal bilayer domains are detected. Frictional coefficients are essentially the same for both phases, indicating that interaction of the tip with phospholipid headgroups is predominant. High friction is observed at holes in the bilayer as well as in scan windows created by applying high load forces and velocities to a certain area on the

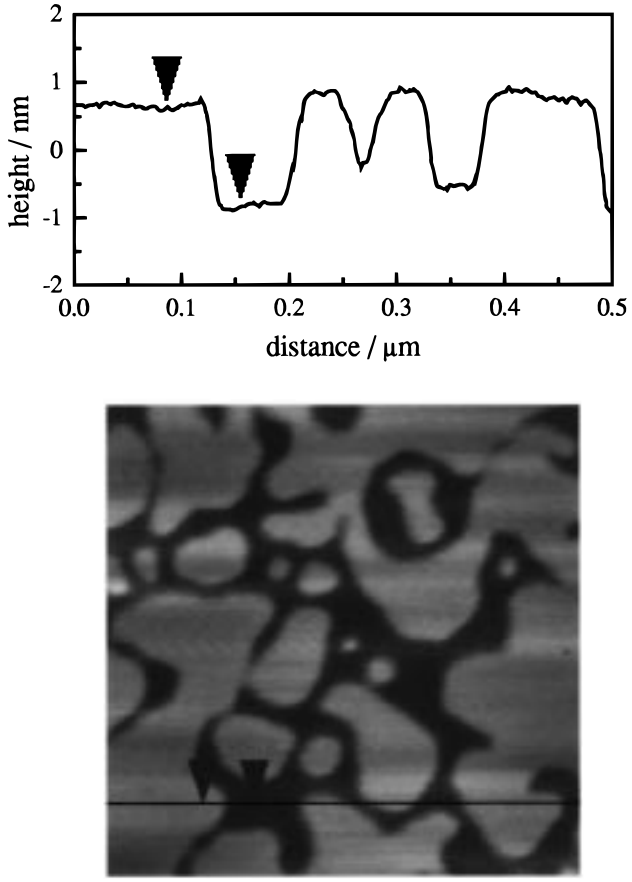

FIGURE 7: Height profile of a DPPC bilayer consisting of $L_{\beta'}$ and L_βI domains. Samples were prepared as described in Materials and Methods. The height difference of the phases obtained from the average of 50 SFM measurements is 1.5 ± 0.2 nm. The thickness of the interdigitated domains is therefore 4 nm with respect to the mica surface, including a thin layer of water between the support and membrane.

sample, which is consistent with the strong interaction of the hydrophilic tip and hydrophilic mica surface giving rise to high frictional forces.

Notably, no transition to the normal gel phase $L_{\beta'}$ could be observed, although the temperature was kept below the premelting temperature of the DPPC system during imaging. The domain structure was stable over more than 10 h at room temperature, consistent with the findings of Mou et al. (*3*, *20*), who imaged interdigitated domains of DPPC and DSPC bilayers on mica induced by ethanol at room temperature.

DISCUSSION

Data presented in this study converge upon the conclusion that interaction of the γ_1-peptide with gel phase lipid bilayers results in the formation of an interdigitated membrane phase. Scanning force microscopy with solid supported DPPC bilayers has revealed the peptide-dependent formation of compressed membrane domains coexisting with normal bilayer regions. A reduction in membrane thickness is a hallmark of lipid interdigitation; thus, the surface height information that can be accessed by SFM is compelling evidence for the L_βI phase. Indeed, SFM has previously been applied to the examination of the well-established phenomenon of ethanol-induced lipid interdigitation (*15*, *18*, *40*) and was demonstrated (*20*) to be a much more sensitive method than X-ray diffraction for detecting changes in bilayer thickness. The strikingly similar phase separation and bilayer height profiles observed by SFM in mica-supported γ_1-bilayers (Figure 6) and ethanol-treated bilayers (Supporting Information) provide a solid foundation to the notion that γ_1 induces interdigitation in gel phase DPPC bilayers. The height difference between the compressed lipid phase and the $L_{\beta'}$ phase in the ethanol-treated bilayer is approximately 1.6 ± 0.1 nm, in good agreement with the height differences observed in the γ_1-treated bilayer.[3]

Structural investigation of ethanol-induced interdigitated DPPC bilayers has shown that lipids in the L_βI phase are much more closely packed (*10*) and are therefore also less mobile. Thus, further evidence for the ability of γ_1 to induce the L_βI phase was gathered from pyrene excimer fluorescence experiments demonstrating that lipid mobility in PyrPC-doped DPPC vesicles was reduced upon treating the liposomes with peptide. Additionally, a comparison of SFM images of ethanol- and γ_1-charged bilayers reveals that γ_1 is much more efficient at inducing phase transformation than ethanol. This trend is also reflected in excimer fluorescence experiments, which reveal a much steeper dependence of lipid mobility of γ_1 than on ethanol. It is reasonable to expect that the peptide is more efficient at inducing a lipid phase change than ethanol, as the peptide presents a much larger interaction area to the bilayer than does ethanol, thus binding and affecting more lipids per mole of additive with lower entropic cost. The lack of a cooperative dependence of *E*/*M* on γ_1 may be rooted in the inherent differences between ethanol and peptide. When initial interdigitation occurs in the bilayer, the terminal methyl groups of the acyl chains are exposed to aqueous environs near the headgroups of the opposing monolayer. These hydrophobic groups represent binding sites for subsequent ethanol molecules to stabilize phase separation by filling in the interstitial space formed between headgroups (*41*). The binding of ethanol leads to further interdigitation and the baring of additional binding sites, establishing a positive feedback cycle that results in the sigmoidal shape (*10*) of the *E*/*M* dependence on ethanol concentration (Figure 4). Titration calorimetry experiments (*9*) have established that the γ-peptide fragment has an affinity for both phosphocholine and phosphoglycerol headgroups as well as for the hydrophobic lipid matrix, and therefore, in contrast to the case for ethanol, interdigitation does not appreciably affect the number of γ_1 binding sites. Consequently, induction of the L_βI phase is cooperative, although the decrease in the excimer/monomer fluorescence ratio is not.

The nature of the binding interaction was clarified by CD, ATR-IR, and fluorescence experiments. Fluorescence studies in which the dielectric environment of Trp-4 on γ_1 was monitored revealed that the peptide was only able to insert into DPPC bilayers when incubated with lipid above the T_m. Moreover, γ_1 incorporation was found by CD to be concomitant with a random coil to α-helix transition in peptide secondary structure. ATR-IR investigations with peptide−DPPC multibilayers provided information about peptide

[3] The thickness of the water layer between the membranes and the solid support currently is a matter of speculation. Assuming that the water layer is equally thick between both the L_βI and $L_{\beta'}$ phases and the mica surface, a 1 nm thick water layer is expected.

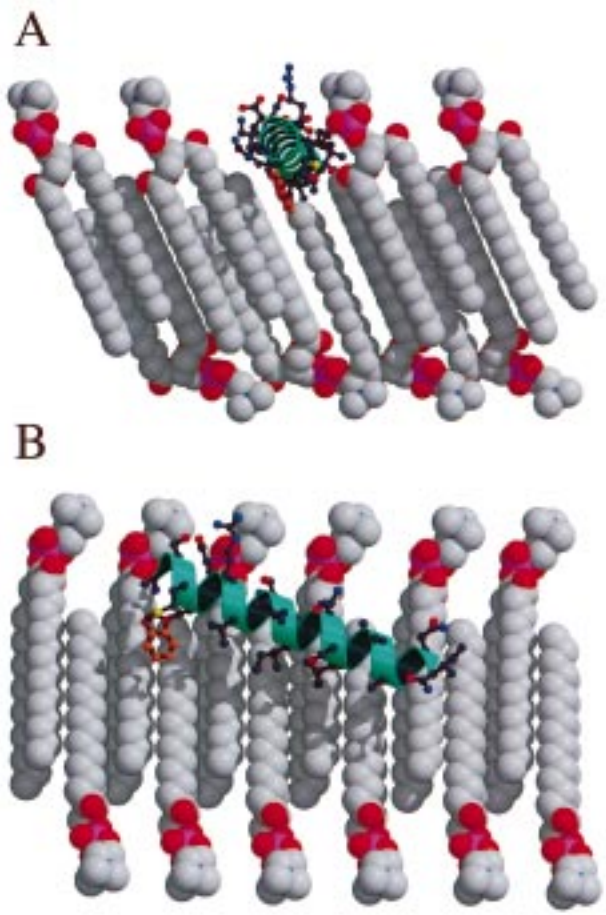

FIGURE 8: Proposed model of γ_1-induced interdigitation in DPPC membranes. The images were generated using the MOLSCRIPT interface with Raster3D (*44*, *45*). (A) Depiction of the peptide, represented as a helix, imbedded in an interdigitated bilayer, viewed along the plane of the helical axis and the surface normal and (B) viewed perpendicular to the helical axis. This schematic illustration emphasizes the 68° tilt of the peptide and the 30° angle of the lipids with respect to the surface normal, as well as the burial of the hydrophobic face of the helix in the hydrocarbon interior. The following color code is used for lipids, rendered as CPK structures with phosphorus atoms shown being purple, oxygen atoms red, nitrogen atoms blue, and carbon atoms gray. For the γ_1-peptide, the helical backbone is green, with side chains rendered as ball-and-stick diagrams and colored with carbon atoms being deep purple, oxygen atoms red, nitrogen atoms blue, sulfur atoms yellow, and the tryptophan indole orange. Hydrogens have been omitted for clarity.

orientation that places the helical axis of the peptide at a 68° angle from the surface normal, and 38° from the lipid chain axis. Together, the above data form a clear picture of the peptide−lipid interaction: γ_1 burrows between lipid headgroups in the fluid phase, and hydrocarbon solvation of γ_1's hydrophobic side chains drives helical organization. Upon cooling to the gel phase, γ_1 is retained by the bilayer in a helical conformation. Assuming a linear helix, one can envision the peptide as a rod lying roughly flat in a lipid carpet with its hydrophobic face buried in the hydrocarbon matrix and its hydrophilic face solvent-exposed, as is typical for many amphiphilic peptide helices (Figure 8). In contrast to X-ray diffraction results (*15*), ATR-IR data did not indicate a lipid chain tilt angle of 0° upon interdigitation; rather, as shown in Figure 8, the usual tilted orientation was found. The lipid orientation may be dependent on the degree of phase separation; since X-ray diffraction techniques can only identify a fully interdigitated phase, the lipid orientation inferred from X-ray data may not apply to lipid systems such as those detected by SFM with coexisting $L_{\beta'}$ and $L_\beta I$ phases. If one invokes a 0° lipid tilt at the boundary between normal bilayer and interdigitated phases, molecular modeling indicates that it becomes impossible to pack lipids in a planar fashion without large transmembrane cavities, rendering this assembly scenario unlikely. This current model we have proposed for γ_1 interacting with DPPC meets the requirements for interdigitation put forth by Slater and Huang (*18*).

Full interdigitation can be induced by a variety of amphiphilic substances. In addition to small amphiphiles such as short chain alcohols, polyols, and anesthetics, it is well-established that positively charged peptides such as polymyxin (*42*) and myelin basic protein (*43*) are capable of inducing interdigitation in negatively charged lipid bilayers consisting of DPPG. More recently, Boggs and Tümmler have demonstrated (*4*) that polymyxin also causes interdigitation in gel phase POPG membranes and motionally restricts spin-labels in gel phase lipid extracts of the Gram-negative bacteria *Pseudomonas aeruginosa*. However, whereas incubation above the T_m is necessary for γ_1 to effect the phase transition with PC lipids, the electrostatic interaction between the polycationic PMB and the polyanionic DPPG surface may be sufficient to allow insertion. From studies with PC lipids, it is apparent that a critical factor in determining whether the $L_\beta I$ phase will form is the degree to which membrane insertion occurs (*19*); agents which insert in a transmembrane fashion do not induce interdigitation.[4] Active molecules are those which cause lateral headgroup separation by localizing the headgroup−solvent interface rather than the bilayer interior. This insertion creates a local disruption of gel phase bilayer packing in one monolayer leaflet, which can best be addressed with a compensating transition to the interdigitated phase. Thus, the fact that γ_1 causes an $L_{\beta'}$ to $L_\beta I$ transition implies that the viral capsid γ-peptide inserts shallowly into membranes, initially perturbing only the outer monolayer.

This study has demonstrated the capability of the N-terminal part of the flock house virion capsid cleavage protein to drastically manipulate lipid phase morphology. Since interdigitation is restricted to gel phase membranes and biomembranes are typically fluid, the biological importance of the $L_\beta I$ phase is unclear.[5] However, because of established prerequisites of $L_\beta I$ phase formation, one can draw further inferences about the mode of γ_1 binding to the bilayer; this is the true value of these studies. It is not unreasonable to extrapolate the insertion properties of γ_1 in gel phase lipids to the analysis of interactions between γ_1 and fluid phase lipids (*9*). In doing so, one sees that under the experimental conditions, γ_1 cannot be incorporated as a transmembrane bundle that creates a localized disturbance, but rather, it interacts more potently in a fashion that can more effectively disrupt both gel and fluid bilayers. Indeed, it has been demonstrated that interdigitation results in a marked increase in the extent of transmembrane passage of large hydrophilic

[4] However, hydrophobic mismatch may cause local bilayer−bilayer depressions (*3*).

[5] It has been suggested that metastable gel and fluid phase separation in biological membranes is possible, thus allowing the possibility of interdigitation in biomembranes (*4*).

molecules (*11*, *12*). Together with fluid phase studies, this work adds an additional dimension to the high membrane activity of the FHV cleavage peptide fragment. These results augur well for the hypothesis that the cleavage peptide has a role in permeabilizing target membranes in the transfection process of the flock house virus.

SUPPORTING INFORMATION AVAILABLE

CD spectra of the γ_1-peptide under various conditions, the fluorescence spectrum of PyrPC, lateral force microscopy images of the γ_1-peptide in DPPC, scanning force microscopy images of DPPC in the presence of ethanol, and height profiles of interdigitated domains and noninterdigitated domains in the vicinity of a scan window. This material is available free of charge via the Internet at http://pubs.acs.org.

REFERENCES

1. Babin, Y., D'Amour, J., Pigeon, M., and Pezolet, M. (1987) *Biochim. Biophys. Acta 903*, 78−88.
2. Theretz, A., Ranck, J. L., and Tocanne, J. F. (1983) *Biochim. Biophys. Acta 732*, 499−508.
3. Mou, J., Czajkowsky, M., and Shao, Z. (1996) *Biochemistry 35*, 3222−3226.
4. Boggs, J. M., and Tuemmler, B. (1993) *Biochim. Biophys. Acta 1145*, 42−50.
5. Schneemann, A., Reddy, V., and Johnson, J. E. (1998) *Adv. Virus Res. 50*, 381−446.
6. Fisher, A. J., and Johnson, J. E. (1993) *Nature 361*, 176−179.
7. Cheng, R. H., Reddy, V. S., Olson, N. H., Fisher, A. J., Baker, T. S., and Johnson, J. E. (1994) *Structure 2*, 271−282.
8. Kaesberg, P., Dasgupta, R., Sgro, J. Y., Wery, J. P., Selling, B. H., Hosur, M. V., and Johnson, J. E. (1990) *J. Mol. Biol. 214*, 423−435.
9. Bong, D. T., Steinem, C., Janshoff, A., Johnson, J. E., and Ghadiri, M. R. (manuscript in preparation).
10. Simon, S. A., and McIntosh, T. J. (1984) *Biochim. Biophys. Acta 773*, 169−172.
11. Komatsu, H., and Okada, S. (1995) *Biochim. Biophys. Acta 1237*, 169−175.
12. Komatsu, H., and Okada, S. (1996) *Biochim. Biophys. Acta 1283*, 73−79.
13. Auger, M., Jarrell, H. C., Smith, I. C. P., Siminovitch, D. J., Mantsch, H. H., and Wong, P. T. T. (1988) *Biochemistry 27*, 6086−6093.
14. Maruyama, S., Hata, T., Matsuki, H., and Kaneshina, S. (1997) *Biochim. Biophys. Acta 1325*, 272−280.
15. McIntosh, T. J., McDaniel, R. V., and Simon, S. A. (1983) *Biochim. Biophys. Acta 731*, 109−114.
16. Kinoshita, K., and Yamazaki, M. (1996) *Biochim. Biophys. Acta 1284*, 233−239.
17. Hao, Y.-h., Xu, Y.-m., Chen, J.-w., and Huang, F. (1998) *Biochem. Biophys. Res. Commun. 245*, 439−442.
18. Slater, J. L., and Huang, C.-H. (1988) *Prog. Lipid Res. 27*, 325−359.
19. Rowe, E. S., and Campion, J. M. (1994) *Biophys. J. 67*, 1888−1895.
20. Mou, J., Yang, J., Huang, C., and Shao, Z. (1994) *Biochemistry 33*, 9981−9985.
21. Galla, H. J., and Hartmann, W. (1980) *Chem. Phys. Lipids 27*, 199−219.
22. Schnolzer, M., Alewood, P., Jones, A., Alewood, D., and Kent, S. B. H. (1992) *Int. J. Pept. Protein Res. 40*, 180−193.
23. Bohm, G., Muhr, R., and Jaenicke, R. (1992) *Protein Eng. 5*, 191−195.
24. Dalmas, B., Hunter, G. J., and Bannister, W. H. (1994) *Biochem. Mol. Biol. Int. 34*, 17−26.
25. Andrack, M. A., Chacon, P., Merelo, J. J., and Moran, F. (1993) *Protein Eng. 6*, 383−390.
26. Harrick, N. J. (1967) *Internal Reflection Spectroscopy*, Interscience, New York.
27. Fringeli, U. P., and Gunthard, H. H. (1981) *Membrane Spectroscopy*, Springer-Verlag, New York.
28. Fraser, R. D. B. (1958) *J. Chem. Phys. 28*, 1113−1115.
29. Tamm, L. K., and Tatulian, S. A. (1997) *Q. Rev. Biophys. 30*, 365−429.
30. Fraser, R. D. B. (1953) *J. Phys. Chem. 21*, 1511−1513.
31. Frey, S., and Tamm, L. K. (1991) *Biophys. J. 1071*, 123−148.
32. Brian, A. A., and McConnell, H. M. (1984) *Proc. Natl. Acad. Sci. U.S.A. 81*, 6159−6163.
33. Di Transcesco, V., Garnier, J., and Munson, P. J. (1996) *Protein Sci. 5*, 106−113.
34. Levin, J. M., Robson, B., and Garnier, J. (1986) *FEBS Lett. 205*, 303−308.
35. Chung, L. A., Lear, J. D., and DeGrado, W. F. (1992) *Biochemistry 31*, 6608−6616.
36. Bartucci, R., Pali, T., and Marsh, D. (1993) *Biochemistry 32*, 274−281.
37. Bartucci, R., Montesano, G., and Sportelli, L. (1997) *Appl. Magn. Reson. 12*, 41−52.
38. Hresko, R. C., Sugar, I. P., Barenholz, Y., and Thompson, T. E. (1986) *Biochemistry 25*, 3813−3823.
39. Shao, Z., and Yang, J. (1995) *Q. Rev. Biophys. 28*, 195−251.
40. McDaniel, R. V., McIntosh, T. J., and Simon, S. A. (1983) *Biochim. Biophys. Acta 731*, 97−108.
41. Adachi, T., Takahashi, H., Ohki, K., and Hatta, I. (1995) *Biophys. J. 68*, 1850−1855.
42. Boggs, J. M., and Rangaraj, G. (1985) *Biochim. Biophys. Acta 816*, 221−233.
43. Boggs, J. M., Stamp, D., and Moscarello, M. A. (1982) *Biochemistry 21*, 1208−1214.
44. Kraulis, P. J. (1991) *J. Appl. Crystallogr. 24*, 946−950.
45. Merritt, E. A., and Murphy, M. E. P. (1994) *Acta Crystallogr. D50*, 869−873.

BI982976I